European Journal of Mechanics B/Fluids 29 (2010) 224–235

Contents lists available at ScienceDirect

European Journal of Mechanics B/Fluids

journal homepage: www.elsevier.com/locate/ejmflu

The effect of inlet pulsations on the backward-facing step flow

J. Tihon [a,*], V. Pěnkavová [a], M. Pantzali [b]

[a] Institute of Chemical Process Fundamentals, Academy of Sciences of the Czech Republic, Rozvojova 135, 16502 Prague, Czech Republic

[b] Chemical Engineering Department, Aristotle University of Thessaloniki, Greece

ARTICLE INFO

Article history:
Received 22 December 2008
Received in revised form
16 July 2009
Accepted 4 February 2010
Available online 12 February 2010

Keywords:
Flow separation and reattachment
Backward-facing step
Flow forcing
Wall shear stress
Electrodiffusion method

ABSTRACT

This experimental study of backward-facing step flow is focused on the transient flow regime (Re_h from 30 to 1800). The electrodiffusion technique is applied to measure the wall shear rate in a water channel with the most common expansion geometry ($ER = 2$). The direction-sensitive wall probes are able to recognize the individual regions of flow separation and reattachment behind the step. The bottom and roof wall shear rate profiles are obtained under steady and pulsatile flow conditions at the inlet. The near-wall extent of primary (mean reattachment length) and secondary (corner and roof eddy location) flow-recirculation zones is determined from these profiles. The high level of wall shear rate is observed inside the reverse flow regions even at moderate Reynolds numbers. The spectral analysis of natural flow fluctuations reveals that the low frequencies characterized by $St_h \sim 0.15$ dominate the reattachment region. The inlet flow pulsations affect strongly the overall flow structure behind the step. Up to 80% reduction of the reattachment length is achieved by applying flow pulsations at the most effective frequency. Two flow instability modes are found to be important to control this frequency: the "step mode" dominates the laminar flow regime, whereas the "shear layer mode" prevails at the transient flow conditions. The frequency of "step mode" coincides with the scaling recently suggested for the global instability of backward-facing step flows.

1. Introduction

The backward-facing step flow represents a popular configuration to study flow separation and reattachment. However, this simple geometry produces the flow with a curved separated shear layer and exhibits a great deal of complexity: development of large vortex structures in the free shear layer, generation of flow disturbances due to the shear layer/reattachment wall interaction, feedback effect of near-wall flow perturbations on flow separation through the separation bubble, formation of the reverse flow, and slow recovery of the reattached shear layer to an equilibrium state.

The experimental studies on backward-facing step flow have been mainly focused on the laminar and developed turbulent regimes, when the flow downstream the step remains predominately 2D. The first systematic measurements covering also the transition flow regime were done by Armaly et al. [1] for the channel geometry with the expansion ratio $ER = 2$. An unsteady flow pattern with additional regions of flow separation downstream (a recirculation region at the roof wall, and a secondary flow-recirculation region at the bottom wall) was observed for moderate Reynolds numbers. The transient flow regime was found to be 3D in character and susceptible to oscillations caused by interactions between the shear layer and recirculation flow.

There are two qualitatively different sources of three-dimensionality of the backward-facing step flow: the influence of channel geometry (extrinsic sidewall effect) and the action of hydrodynamics (intrinsic flow instability). The existence of sidewall-induced recirculation regions, which are important mainly in channels with small aspect ratios, was identified in velocity measurements by Armaly et al. [2] and Nie and Armaly [3] and numerical simulations by Williams and Baker [4], Chiang and Sheu [5], Biswas et al. [6], and Kitoh et al. [7]. The investigation of the linear stability of backward-facing step flow has been based mainly on numerical simulations. The numerical results by Kaiktsis et al. [8] suggested the existence of a local convective instability for $Re_h > 350$, with the onset of flow three-dimensionality occurring at the boundary between the recirculation zones and the bulk flow. Barkley et al. [9] found for the 3D destabilization of the steady, 2D flow over a backward-facing step a critical value of $Re_h \sim 500$. Moreover, the existence of 3D flow structures was reported at even lower Reynolds numbers. Beaudoin et al. [10] observed experimentally stationary flow structures with a "mushroom-like" shape and a spanwise periodicity at $Re_h \sim 100$. Recently, the global stability analysis (see e.g. [11–14]) has revealed the existence of

* Corresponding author. Tel.: +420 220390250; fax: +420 220920661.
E-mail address: tihon@icpf.cas.cz (J. Tihon).

0997-7546/$ – see front matter © 2010 Elsevier Masson SAS. All rights reserved.
doi:10.1016/j.euromechflu.2010.02.001

Notations

a_e	relative amplitude of the inlet flow pulsations $= u_e/U$
$b_{1,2}$	calibration constants of the electrodiffusion probe (see Eqs. (2) and (3))
AR	spanwise aspect ratio $= W/h$
c_o	concentration of the active ions (kmol/m^3)
c_f	skin friction coefficient $= 2\bar{s}_w\nu/U^2$
$c_{f,\min}$	skin friction magnitude inside the flow-recirculation region $= 2\bar{s}_{w,\min}\nu/U^2$
D	diffusion coefficient of the active ions (m^2/s)
ER	expansion ratio of the channel $= 1 + h/H$
f	frequency of natural flow fluctuations (Hz)
f_e	frequency of the forced flow pulsations (Hz)
f_{opt}	frequency of the most effective flow forcing (Hz)
F	Faraday constant $= 9.648 \times 10^7$ (C/kmol)
h	height of the step (m)
H	upstream height of the channel (m)
I	current signal from the single strip probe (A)
I_1	current through the upstream probe segment (A)
I_2	current through the downstream probe segment (A)
$k_{1,2}$	calibration constants of the electrodiffusion probe (see Eqs. (2) and (3))
l	downstream length of the single strip probe (m)
n	number of electrons involved in the redox reaction
Re_h	Reynolds number based on the step height $= Uh/\nu$
s_w	wall shear rate $= \partial u_x/\partial y\|_{y=0\ or\ (h+H)}$ (1/s)
s_{wo}	wall shear rate in the channel under fully developed flow conditions (1/s)
$\bar{s}_w$	time-averaged value of the wall shear rate (1/s)
$\tilde{s}_w$	magnitude of wall shear rate fluctuations (r.m.s. value) (1/s)
$\tilde{s}_{w,\max}$	maximum local value of $\tilde{s}_w$ (1/s)
St_h	Strouhal number based on the step height $= fh/U$
$St_{h,e}$	Strouhal number based on the step height and the forcing frequency $= f_e h/U$
St_θ	Strouhal number based on the separation momentum thickness $= f\theta/U_{\max}$
$St_{\theta,e}$	Strouhal number based on the separation momentum thickness and the forcing frequency $= f_e\theta/U_{\max}$
t	time (s)
u_e	amplitude of velocity fluctuations due to the inlet flow pulsations (m/s)
U	mean velocity in the upstream channel section (m/s)
$U_{\max}$	maximum velocity in the upstream channel section under the steady flow (m/s)
w	probe segment width (m)
W	width of the channel (m)
W_{ss}	power spectral density function of wall shear rate fluctuations (1/s)
x	longitudinal coordinate (distance from the step) (m)
x_c	length of the corner eddy (m)
$x_{\max}$	position of $\tilde{s}_{w,\max}$ (m)
x_p	position of the negative peak value of $\bar{s}_w$ (m)
x_r	reattachment length (m)
x_{ro}	reattachment length corresponding to steady inlet flow conditions (m)
x_{ts}	position of the flow separation at the roof wall (m)
x_{tr}	position of the flow reattachment at the roof wall (m)
y	normal coordinate (distance from the bottom wall) (m)
δ	boundary layer thickness (m)
γ_p	reverse-flow time fraction in the near-wall region
θ	separation momentum thickness $= \int_h^{h+H/2} u_x/U_{\max}(1 - u_x/U_{\max})\mathrm{d}y$ (m)
ν	kinematic viscosity of the fluid (m^2/s)
ρ	fluid density (kg/m^3)

regions of the transient growth/convective instability in backward-facing step flows at low Reynolds numbers.

Many studies have been performed to understand unsteady character of the backward-facing step flow. A general trend observed in power spectra of flow fluctuations downstream the separation point is the energy redistribution towards low frequencies (see e.g. [15]). Three typical instabilities have been identified in the separated flow region past a backward-facing step:

- The frequency of a convective Kelvin–Helmholtz instability, which originates in the natural rolling-up of the separated shear layer, scales with a characteristic length of the initial shear layer. This "*shear layer mode*" of instability can be characterized by a Strouhal number based on the momentum thickness with a typical value of $St_\theta \sim 0.012$ (see e.g. [16]).
- The process of subsequent vortex merging leads to the appearance of the so-called "*step mode*" instability. For this instability mode the relevant frequency scaling is based on the size of recirculation region (the step height h, downstream channel height $H + h$ or reattachment length x_r are usually applied as the characteristic lengths). If the Strouhal number St_h based on the step height is considered, the spectral analysis of natural flow fluctuations inside the reattachment zone provides values of $St_h = \mathcal{O}(10^{-1})$ (see e.g. the spectra presented by Roos and Kegelman [17] and Berbee and Ellzey [18]).

  Wee et al. [19] applied the linear stability analysis to investigate the origin of self-sustained fluctuations in backward-facing step flows. Their results suggest that the eddy shedding phenomena are supported by the absolutely unstable flow regime in the recirculation zone with the dominant frequency tuned in to $St_h \sim 0.07$. The wall pressure oscillations with the same dominant frequency were experimentally observed by Lee and Sung [20] within the primary flow-recirculation zone.

  The global stability analysis provides for the frequency of transient packets of optimum flow perturbations the similar estimate $St_h = \mathcal{O}(10^{-1})$. However, the frequency scaling suggested by Blackburn et al. [12] and Marquet et al. [14] is based on the parameters (the mean velocity and the channel height) measured downstream the step.
- The unsteady fluid exchange between the separated shear layer and the recirculation region results in the inception of a low-frequency instability experimentally identified as the "*flapping mode*". It is indicative of a growth-decay cycle of the separation bubble and has a characteristic frequency of $St_h = \mathcal{O}(10^{-2})$, i.e. one order lower than the "step mode".

The role of forced perturbations in controlling the flow field behind the backward-facing step was first studied by Bhattacharjee et al. [15] and Roos and Kegelman [17]. They observed that the perturbation at discrete frequencies (for $St_{h,e}$ from 0.2 to 0.4) increases the growth rate of shear layer and thus shifts the reattachment point upstream. Since then many different passive and active control methods have been used to affect the momentum transport across the shear layer. For example, an oscillating flap at the separation position was applied by Roos and Kegelman [17], acoustic excitation above the step edge by Bhattacharjee et al. [15], upstream cavities or rods by Isomoto and Honami [21], and blowing/suction at the step edge by Chun and Sung [22] and Yoshioka et al. [23].

A general consensus on the most effective forcing for turbulent flow separation is achieved for the similarity based on a value of $St_{\theta,e} \sim 0.01$, i.e. corresponding to the vortex shedding frequency of the unforced flow (see e.g. [22]). The reattachment length reduction achieved under these turbulent flow conditions is somewhere between 20% and 30%. The numerical studies on the control of turbulent flow separation provided similar results (see e.g. [24–26]).

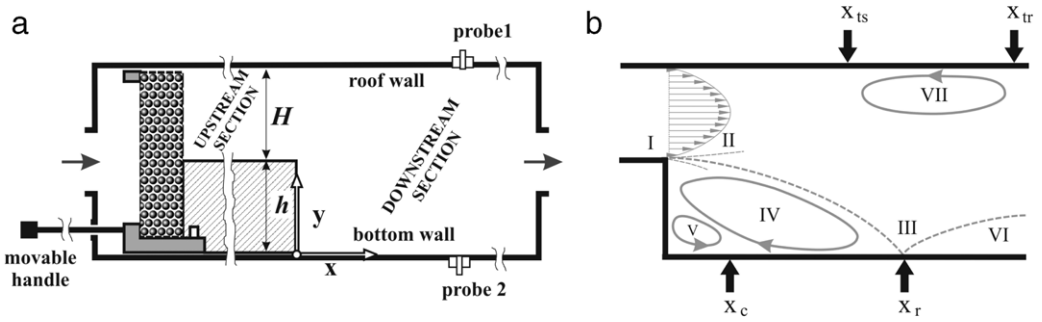

Fig. 1. Backward-facing step apparatus (a) with the flow pattern (b) inside: inlet velocity profile (I), separated shear layer (II), reattachment zone (III), recirculation region (IV), corner eddy (V), redeveloping channel flow (VI), and roof eddy (VII).

There are only few experimental studies dealing with the flow separation control at relatively low Reynolds numbers achieved in water channels. Yoshioka et al. [23] found out (for turbulent inflow, $Re_h \sim 3700$) the maximum shortening of x_r (about 30%) at the forcing frequency corresponding to $St_{h,e} \sim 0.2$, whereas Chun and Sung [27] obtained (for laminar inflow, $Re_h \sim 1200$) a stronger effect of excitation resulting at $St_{h,e} \sim 0.48$ in a more important reduction of x_r (about 70%). Another low Reynolds number study carried out at laminar inflow conditions ($Re_h = 1480$ and 3000) was done by Wengle et al. [28]. The most effective forcing frequency observed in their low-speed wind tunnel for two different step heights ($ER = 1.04$ and 1.09), was not scaled with the step height ($St_{h,e} \sim 0.18$ and 0.36, respectively), but with the momentum thickness of the initial boundary layer ($St_{\theta,e} \sim 0.01$). The maximum level of reattachment length reduction (55% and 30%, respectively) was thus again achieved for the forcing at the shear layer instability mode.

The present experimental study of backward-facing step flow is mainly focused on the transient flow regime (Re_h from 30 to 1800) in the most common channel geometry ($ER = 2$). Our objective is to investigate the near-wall flow organization by the mapping of fluctuating wall shear rate downstream the step. The electrodiffusion diagnostics of the near-wall flow is proved to be an efficient measuring technique for this purpose. First, the unsteady flow pattern with several flow separation regions observed behind the step under steady inlet flow conditions is explored and analyzed. After that, the effect of inlet flow pulsations on the overall flow structure is studied with the aim to find out the most effective mode of forcing and also to assess the role of different instability modes acting at low and moderate Re_h.

2. Experimental apparatus and procedure

2.1. Experimental set-up

The investigation of backward-facing step flow is carried out in an experimental channel as schematically shown in Fig. 1. Its basic part is a rectangular channel (0.25 m in width, 0.02 m in height, and 2 m in length) made of Plexiglass. A rectangular block of Plexiglass having a thickness of $h = 10$ mm is movably installed into this channel to create a backward-facing step, which abruptly changes the channel height from $H = 10$ mm (upstream the step) to $H + h = 20$ mm (downstream the step). The channel geometry is characterized by the expansion ratio of $ER = 1 + h/H = 2$ and the spanwise aspect ratio of $AR = W/h = 25$. A sliding part of the apparatus consists of a handle, a calming section, and the step block joined together. The calming flow chamber has a thickness of 25 mm and contains small glass balls 2 mm in diameter. The length of the upstream channel section (1 m) is sufficient to achieve a developed velocity profile at the step edge. Two electrodiffusion probes are located at the channel spanwise centerline 400 mm from the channel outlet. This 40 h distance is sufficient to eliminate any feedback effect of the outlet geometry on the flow structure at the measurement position. The probes are flush mounted into the bottom and roof wall just opposite to each other. Due to movement of the upstream section, the downstream distance between the probe and the step can be gradually changed in the range of x/h from -10 to 60.

Two pumps are used to supply the test fluid from a storage tank (20 l) through a flowmeter into the channel. The gear pump is used for low flow rates (up to 3.5 l/min), the screw one for higher flow rates (up to 25 l/min). To maintain the fluid at a constant temperature (about 21 °C), there is a cooling coil in the storage tank. The mean velocity U in the upstream channel section is adjusted from 0.003 to 0.19 m/s. The corresponding Reynolds number ($Re_h = Uh/\nu$) is ranging from 30 to 1900. The laminar, transient and initial part of turbulent flow regime are thus covered in our experiments. A cylindrical plunger (40 mm in diameter) is mounted into an entrance chamber of the flow loop. Its periodic movement (with a maximum travel of 35 mm) enables us to superimpose low-frequency pulsations (f_e from 0.1 to 3 Hz) on the mean flow at the inlet.

2.2. Electrodiffusion diagnostics of the near-wall flow

The electrodiffusion method (see [29] for a review), based on the measurement of the limiting diffusion current of the ferricyanide ions reduction at a small working electrode, is used to provide information on the wall shear rate behind the step. The current signal I provided by a simple strip probe is controlled by convective diffusion and depending on the wall shear rate s_w according to the following formula

$$I = 0.807\, n F c_0 w l^{2/3} D^{2/3} s_w^{1/3}, \tag{1}$$

where n is the number of electrons involved in the electrochemical reaction, F is the Faraday constant, l is the length of the strip in the mean flow direction, w is its width, c_0 is the bulk concentration of the active ions, and D is their diffusivity in the solution.

The directionally sensitive, double probe is applied with the aim to detect the location of the reattachment point. Its two platinum segments have an identical size (strips with sides of $l = 0.1$ mm and $w = 1$ mm) and are oriented with the longer side w perpendicular to the mean flow direction. An insulating gap between these segments has a thickness of 10 μm. The active segments are glued into a stainless steel tube (diameter of 5 mm) serving as an anode. The near-wall flow reversal can be detected simply by comparing the magnitudes of current signals provided by the upstream (I_1) and downstream (I_2) probe segment. The rear segment (with respect to the actual near-wall flow direction) is in a concentration shade of the front one and thus it gives the lower current signal. The absolute value of wall shear rate is calculated in the same way like in the case of single strip probe just the actually front probe segment is treated. Therefore, if the instantaneous

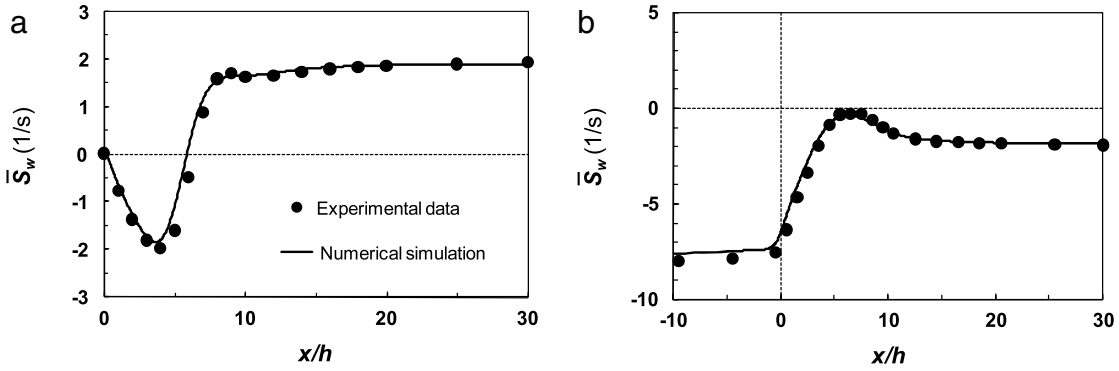

Fig. 2. Wall shear rate profiles measured at (a) the bottom and (b) roof wall under the laminar flow regime, $Re_h = 124$.

flow has the downstream direction, the value of wall shear rate is calculated from the signal of the upstream probe segment $I_1(t)$

$$s_w(t) = (I_1(t)/k_1)^{b_1} \quad \text{for } I_1(t) > I_2(t), \tag{2}$$

whereas if the reverse flow appears in the near-wall region the signal of the downstream probe segment $I_2(t)$ is applied

$$s_w(t) = -(I_2(t)/k_2)^{b_2} \quad \text{for } I_2(t) > I_1(t). \tag{3}$$

The sign convention used in this work for the wall shear rate corresponds to the system of coordinates fixed on the bottom wall, see Fig. 1(a) (negative values for the reverse flow at the bottom wall, positive values for the reverse flow at the roof wall). Steady laminar flow conditions achieved in the upstream section (at $x/h = -10$, roof wall) enable the probe calibration (providing the calibration constant $k_{1,2}$ and $b_{1,2}$ for both the probes). The frequency response of probes is sufficient to depict low-frequency fluctuations of studied backward-facing step flow with a good time resolution. A more detailed discussion on the application of double electrodiffusion probes (especially analysis of their dynamic behavior) can be found in Tihon et al. [30]. The analysis of calibration and steady flow measurements provides the estimates of measuring errors: between 5% and 10% for the wall shear rate measurement (for $\bar{s}_w > 1\ \mathrm{s}^{-1}$) and between 0.1 h (steady flow) and 0.25 h (unsteady flow) for the mean reattachment point localization.

The fluid used for the experiments is water containing equimolar 0.025 M potassium ferro/ferricyanide (as a suitable electrochemical system) and 1 wt% potassium sulfate (as a supporting electrolyte). The solution has a density of $\rho = 1019\ \mathrm{kg/m^3}$ and a kinematic viscosity of $\nu = 1.064\ \mathrm{mm^2/s}$ at a reference temperature of 21 °C. The polarization voltage of −0.8 V is applied to assure that the probes are working under cathodic limiting diffusion current conditions. A home-built electrodiffusion device is used to apply the polarization voltage, to convert currents through the individual probe segments into voltages, and to amplify the resulting signals.

A computer is used to control the electrodiffusion interface and data acquisition. As the backward-facing flow exhibits slow flow fluctuations, the acquisition time between one and two minutes is necessary to obtain statistically valid results. The approximately same time is needed before each new measurement as a pause for the flow stabilization after changing the step position. This fact makes the wall shear stress profile measurements rather time consuming.

2.3. Complementary numerical calculations

To validate the wall shear rate data measured at low Reynolds numbers, the studied laminar backward-facing flow is analyzed by using the commercially available CFD software FLUENT 6.3. The 2D steady flow model corresponds to the experimental channel geometry with $ER = 2$. The computation domain is limited to the distance 20 h upstream and 70 h downstream the step, respectively, with the grid involving in total 136 000 cells.

The finite volume method is used for spatial discretization of the solved differential equations. The discretization schemes PRESTO! and QUICK are applied for pressure and velocity, respectively. The PISO algorithm is implemented to retain pressure–velocity coupling. The parabolic velocity profile is prescribed at the inlet boundary condition. The constant static pressure is prescribed at the outlet boundary.

To compare directly the results of numerical simulations and experimental investigation, the wall shear rate profiles are extracted from the calculated velocity fields. The axial profiles of wall shear rate are then inspected to detect the flow-recirculation regions. The zero local values of wall shear rate determine the positions of flow separation and reattachment points. The numerical calculations are performed for Re_h ranging from 10 to 600.

3. Results and discussion

3.1. Steady flow at the inlet

At low flow rates (for $Re_h < 200$) the backward-facing step flow is found to be steady without significant fluctuations ($\tilde{s}_w/s_{wo} < 0.01$). The wall shear rate is equal to zero at the fixed position of reattachment and the magnitude of wall shear rate fluctuations $\tilde{s}_w$ exhibits a minimum value there. Moreover, the flow is predominantly 2D and therefore the results measured at the channel centerline are in good agreement with the results of our 2D numerical simulations. The typical wall shear rate profiles measured under such steady laminar flow conditions (at $Re_h = 124$) are presented in Fig. 2. The axial profile obtained at the bottom wall (Fig. 2(a)) exhibits a strong negative peak corresponding to flow reversal inside a primary recirculation zone (for x/h from 0 to 6), which is followed by a rapid recovery to the channel flow (for x/h from 6 to 15). The wall shear rate profile measured at the roof wall (Fig. 2(b)) shows that also there the near-wall flow is very close to separation.

As soon as the flow separation at the roof leads to the inception of an eddy, the flow configuration with two flow-recirculation regions becomes unsteady. As seen in Fig. 3 flow fluctuations originated from the separated shear layer are progressively amplified in the recirculation regions. At moderate flow rates (data for $Re_h = 590$ are presented in Fig. 3) the magnitude of fluctuating wall shear rate $\tilde{s}_w$ observed around reattachment is comparable with the wall shear rate level corresponding to the fully developed flow downstream in the channel s_{wo}. The transient regime is characterized by highly unsteady flow having possibly 3D character. This is the reason why the measured profiles of wall shear rate (solid circles) differ from those predicted by

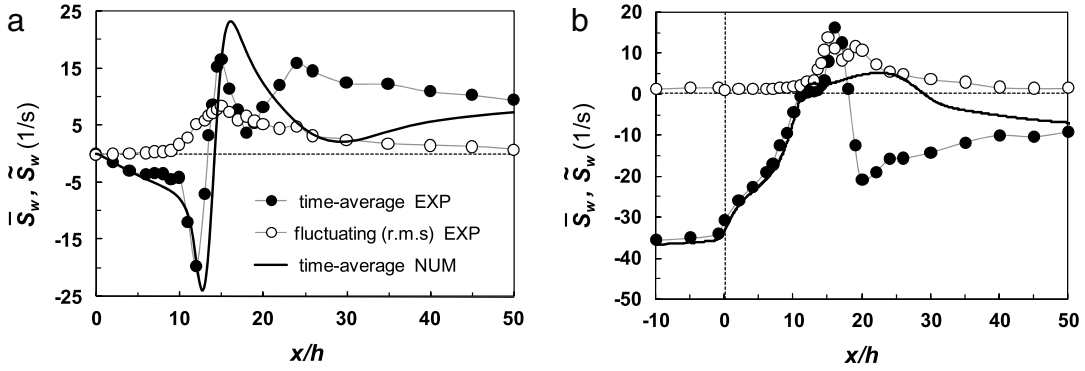

Fig. 3. Wall shear rate profiles at (a) the bottom and (b) roof wall measured (symbols) and computed (2D numerical simulation, thick black lines) for the transient flow regime, $Re_h = 590$.

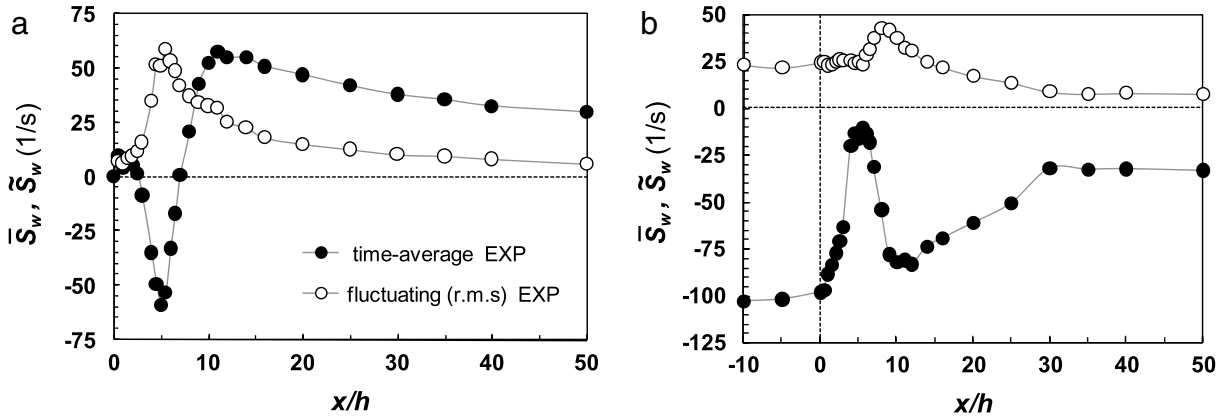

Fig. 4. Wall shear rate profiles measured at (a) the bottom and (b) roof wall after achieving the turbulent flow regime, $Re_h = 1590$.

the steady 2D numerical simulation (thick lines). As the flow reattachment region is that mostly affected by fluctuations (see open circles), the profiles differentiate mainly in the flow recovery region downstream the reattachment. The negative peak on the time-average profile corresponding to the primary recirculation zone is quite asymmetric, with a maximum located very close to the reattachment point (see Fig. 3(a)). As the reattachment point already exhibits irregular low-frequency oscillations, its mean position has to be determined statistically. Both possible methods, i.e. detection of the time-average value of $\bar{s}_w = 0$ or detection of 50% time fraction of the reverse flow in the near-wall region ($\gamma_p = 0.5$), provide practically the same location of reattachment. The profile measured along the bottom wall exhibits another local minimum at $x/h = 18$, but with a positive $\bar{s}_w$ value. A secondary flow-recirculation region, which was previously reported by Armaly et al. [1] for the transient flow regime, is not observed in the present experiment. The profile measured along the roof wall (see Fig. 3(b)) suggests that the recirculation flow inside the roof eddy is quite strong with a back flow of approximately same magnitude as inside the primary flow-recirculation. The maximum level of fluctuations is measured at a location of $x/h \sim 15$, thus in a distance about one step behind the reattachment. The same location of $\tilde{s}_{w,\max}$ is observed at the bottom and roof wall.

The wall shear rate distributions observed after achieving turbulent flow conditions are presented in Fig. 4 (experimental data for $Re_h = 1590$). The profile presented in Fig. 4(a) confirms the existence of two recirculation regions at the bottom wall at high Reynolds numbers. Small positive values of $\bar{s}_w$ just behind the step indicate the presence of a weak corner eddy. Large negative values of $\bar{s}_w$ with a pronounced minimum inside the region of primary recirculation ($|\bar{s}_{w,\min}|/s_{wo} \approx 2$) indicate a strong back flow. The flow

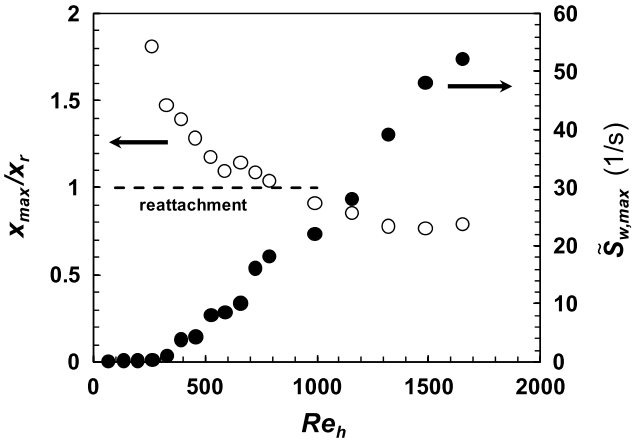

Fig. 5. Variation of the magnitude (value $\tilde{s}_{w,\max}$, solid symbols) and position (with respect to the reattachment point $x_{\max}/x_r$, open symbols) of maximum wall shear rate fluctuations with Re_h.

at the roof wall is still close to separation (see Fig. 4(b)), but the roof eddy disappears in the turbulent flow regime.

As the flow rate in the channel is increased, the magnitude of wall shear rate fluctuations is augmented and at the same time the position of maximum near-wall flow fluctuations at the bottom wall is gradually shifted upstream. It is first located in the region of redeveloping channel flow (in the laminar regime, e.g. at $x/h \sim 20$ for $Re_h = 250$), then shifted just behind the reattachment (in the transient regime, e.g. at $x/h \sim 15$ for $Re_h = 590$), and finally found in front of the reattachment point (in the turbulent regime, e.g. at $x/h \sim 5.5$ for $Re_h = 1590$). Fig. 5 shows that the region of practically steady near-wall flow (for $Re_h < 300$) is followed by

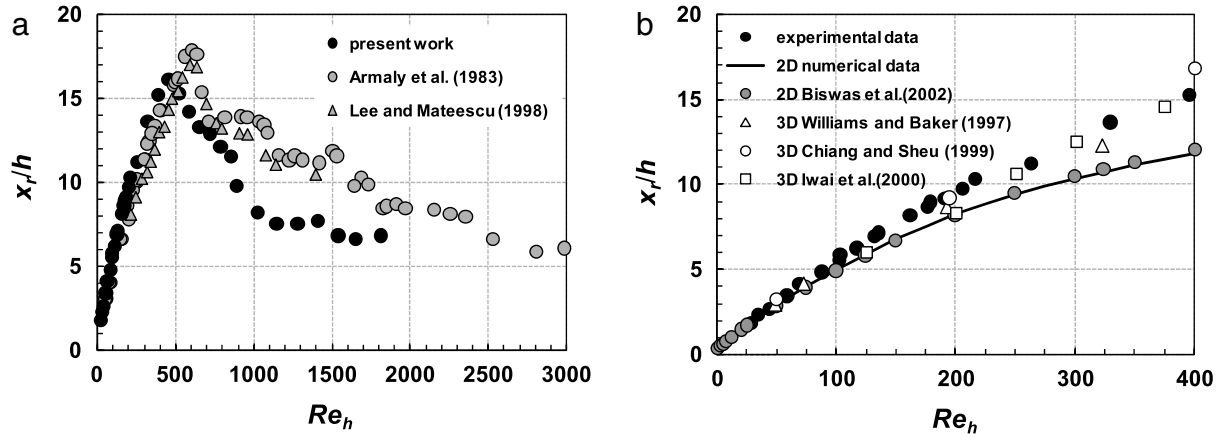

Fig. 6. Dependence of the reattachment length on the Reynolds number: (a) comparison of the recent experimental data, (b) the present experimental results versus the numerical predictions.

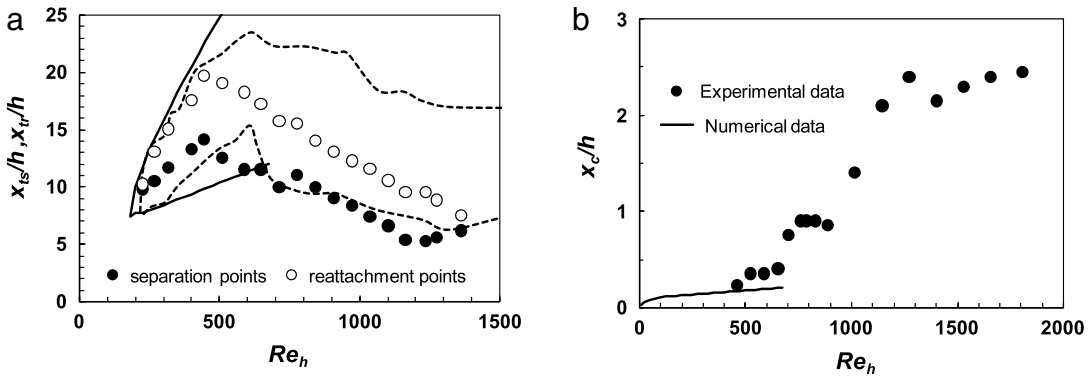

Fig. 7. Extent of the secondary flow-recirculation regions: (a) location of the roof eddy (circle symbols hold for the experimental data, solid lines for the numerical data, and dash lines for the experiment by Armaly et al. [1]), (b) length of the corner eddy.

the region of rapid increasing of $\tilde{s}_{w,\max}$ (for $Re_h > 300$). The local position of maximum wall shear rate fluctuations is observed for $Re_h < 900$ downstream ($x_{\max}/x_r > 1$) and for $Re_h > 900$ upstream ($x_{\max}/x_r < 1$) of the reattachment point (indicated by the dash line in Fig. 5).

Data on the length of primary recirculation zone (reattachment length, x_r) extracted from the measured wall shear rate profiles are presented in Fig. 6. The reattachment length first increases regularly with the Reynolds number, culminates in a peak value under transient flow conditions ($x_{r,\max}/h \sim 16$ for $Re_h \sim 500$), then decreases irregularly and finally reaches a practically constant level in the turbulent regime ($x_{r,turb}/h \sim 7$). As seen in Fig. 6(a) the character of $x_r(Re_h)$ dependence is in a good qualitative agreement with those observed previously for the similar backward-facing step geometries; i.e. for $ER = 1.94$ and $AR = 37$ [1] and for $ER = 2$ and $AR = 40$ [31]. Data agreement in the laminar flow region (for $Re_h < 500$) is very good, but still the measured x_r/h values are slightly sensitive to the individual channel geometries. For the scaling used in Fig. 6, the value of x_r/h decreases with ER (see e.g. numerical analysis by Thangam and Knight [32]) and this ER effect probably causes a small shift between data series by Armaly et al. [1] and Lee and Mateescu [31]. The influence of channel AR (possible 3D flow effects) on the reattachment length is documented in Fig. 6b, where our experimental and 2D numerical data are compared with the results of recent 2D (Biswas et al. [6]) and 3D (Williams and Baker [4] for $AR = 37$, Chiang and Sheu [5] for $AR = 25$, and Iwai et al. [33] for $AR = 16$) numerical simulations. The reattachment length at a centerline position is markedly elongated in channels with finite aspect ratios. According to the numerical results of Chiang and Sheu [5], this elongation effect is strongest just for $AR \sim 20$ (i.e. for the aspect ratio similar to that of our experiment). It can explain why our experiment gives (for Re_h from 200 to 500) little bit higher values of x_r/h. Moreover, the intrinsic flow instability can also play an important role at these moderate Re_h. The experimental data on reattachment length presented in Fig. 6(a) differentiate mainly in the region around $Re_h \sim 1250$. Our results suggest an earlier and more rapid transition to the turbulent flow regime, which probably appears due to the effect of input flow fluctuations originated from very small but not negligible pump pulsations.

The extent of the other two flow-recirculation regions is delimited in Fig. 7. The flow-recirculation at the roof wall appears due to an adverse pressure gradient created by the backward-facing step. It is developed in the laminar regime (at $Re_h \sim 230$), remains in existence throughout the transient regime, and disappears at the beginning of turbulent flow regime (at $Re_h \sim 1400$). The longitudinal extension of the roof eddy is determined by the position of flow separation (x_{ts}, solid circles in Fig. 7(a)) and reattachment (x_{tr}, open circles in Fig. 7(a)) at the roof wall. The measured size of the roof eddy $(x_{tr} - x_{ts})/h$ is shorter than those predicted by our numerical simulations (solid lines) and observed in the experiment by Armaly et al. [1] (dash lines). The position of flow separation at the roof wall seems to be especially sensitive to possible flow perturbations (see the shift in measured and calculated x_{ts} points for Re_h ranging from 200 to 500). The flow separation at the roof wall is always located in front of the position corresponding to the bottom wall reattachment ($x_{ts} < x_r$).

As predicted by numerical calculations (see the solid line in Fig. 7(b)), a small corner eddy exists even at very low Reynolds numbers. It becomes experimentally detectable at sufficiently high

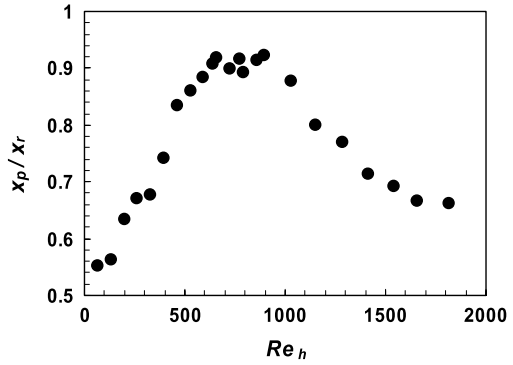

Fig. 8. Variation of the relative position of maximum back flow at the bottom wall with the Reynolds number.

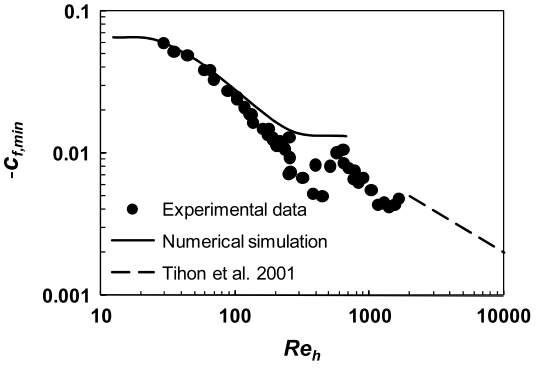

Fig. 9. Peak value of the skin friction coefficient in the reverse flow region as a function of the Reynolds number.

flow rates, when the flow-recirculation inside the eddy is strong enough (as seen in Fig. 7(b) it is the case for $Re_h > 400$). As the volumetric flow rate in the channel is increased, the corner eddy expands and its importance increases rapidly. At turbulent flow conditions the corner eddy length achieves a value of $x_c/h \sim 2.5$ and the ratio of characteristic lengths stabilizes at a value of $x_c/x_r \sim 1/3$ (whereas at $Re_h \sim 500$ a value of $x_c/x_r \sim 1/50$ is observed). The relative importance of corner eddy is strongly dependent on individual experimental conditions (Re_h, ER, AR, inlet flow turbulence) and the recent experimental [34–37] and numerical [38–40] works suggest a range of x_c/x_r from 0.15 to 0.35 for the turbulent flow regime.

The evolution of flow-recirculation structures with an increase of channel flow rates affects also the location x_p of maximum back flow at the bottom wall. The negative peak observed at wall shear rate profiles changes its relative position in respect to the reattachment point (see Fig. 8). At low flow rates the maximum back flow is observed close to the middle of primary recirculation zone ($x_p/x_r \sim 0.5$, see Fig. 2(a)). As the channel flow rate is increased the location of x_p is first shifted towards the reattachment (see Fig. 3(a)), then moved back upstream, and finally stabilized at the position of $x_p/x_r \sim 2/3$ under turbulent flow conditions (see Fig. 4(a)). The position of x_p is placed very close to the reattachment under transient flow conditions ($x_p/x_r \sim 0.9$ for Re_h ranging from 650 to 850).

The local time-averaged skin friction coefficient can be calculated from wall shear rate data by applying the definition formula: $c_f = 2\bar{s}_w \nu / U^2$. The negative peak values of skin friction $c_{f,\min}$, measured inside the primary flow-recirculation zone at the different values of Re_h, are shown in Fig. 9. Experimental data on $c_{f,\min}$ are compared in this figure with the result of our 2D numerical simulation for the steady inlet flow (solid line) and with the empirical relationship suggested for the turbulent flow regime (dashed line, see [35]). A good agreement between the experimental data and numerical prediction is achieved at low Reynolds numbers (for $Re_h < 200$), when steady flow conditions without any flow pulsations are observed behind the step. The skin friction enhancement in the transient flow regime (around $Re_h \sim 500$) is related to sudden shortening of the primary flow-recirculation zone. This change in flow structure affects the process of flow splitting at the reattachment zone and consequently a more important part of the shear layer is deflected upstream to supply the recirculation stream.

The process of flow separation and reattachment induces strong fluctuations in the near-wall flow region. As seen in Figs. 3 and 4, the level of fluctuating wall shear rate is very important even at moderate Reynolds numbers. The power spectra of wall shear rate fluctuations presented in Fig. 10(a) were calculated from the time series measured at a fixed bottom position of $x/h = 14$. Their analysis suggests that the main energy of near-wall flow fluctuations observed around the reattachment point is contained in a low-frequency part of spectrum. The predominant frequency of flow fluctuations can be determined from the location of individual spectral peaks. As the flow rate in the channel grows up, this frequency increases from 0.4 Hz observed at $Re_h = 255$ to 1.4 Hz at $Re_h = 765$. Fig. 10(b) presents one possible approach to spectra normalization. The variance of wall shear rate fluctuations $\mathrm{var}(s_w)$ is applied to obtain a unit integral value under each power spectrum and the characteristic shear rate (U/h) is used to scale the frequency. The values of Strouhal number ($St_h = fh/U$), which characterize the near-wall flow fluctuations observed in our experiment, are ranging from 0.11 to 0.16. The spectral analysis suggests the range of dimensionless frequencies to which our backward-facing step flow is expected to be sensitive also when the pulsations are superposed to the inlet flow.

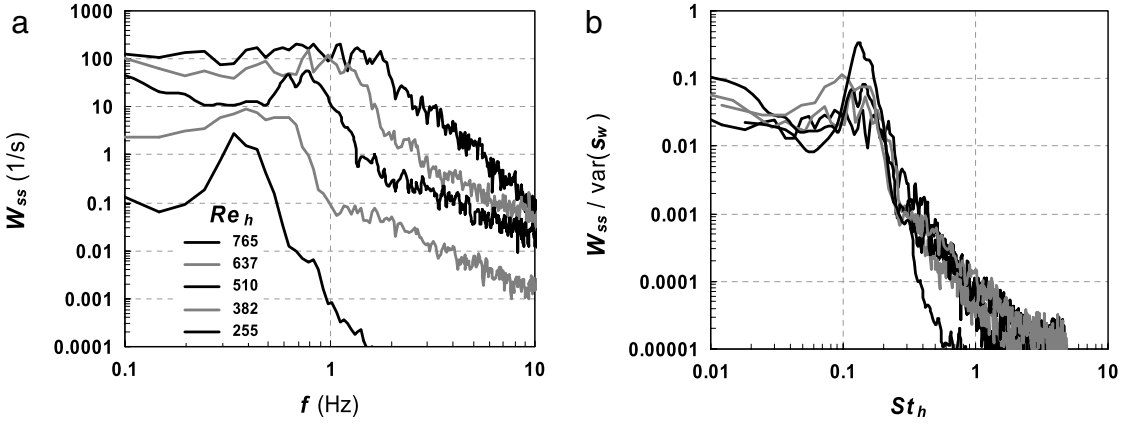

Fig. 10. Power spectra of wall shear rate fluctuations measured at $x/h = 14$: (a) power spectral density function (b) spectra normalization.

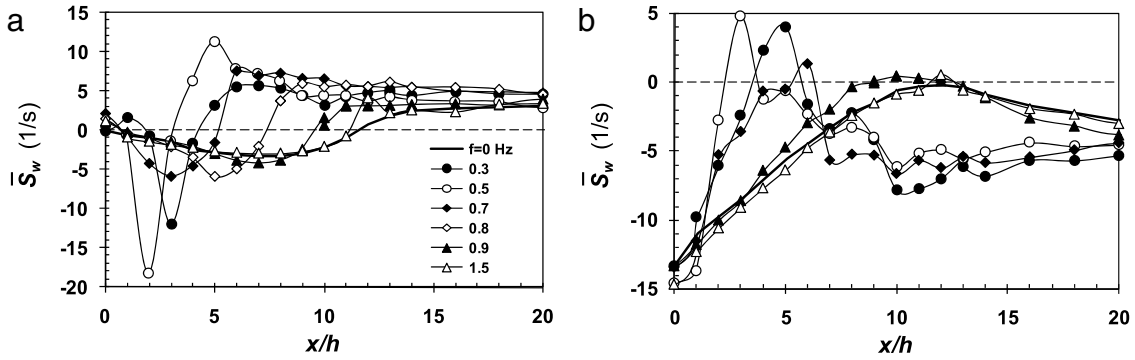

Fig. 11. Wall shear rate profiles measured for the different forcing conditions at (a) the bottom and (b) roof wall. The forcing frequency f_e is varied at the constant forcing amplitude $a_e = 0.3$; for laminar flow separation (at $Re_h = 260$).

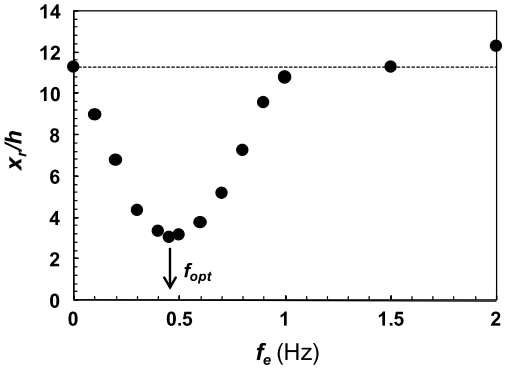

Fig. 12. The reattachment length versus the forcing frequency ($Re_h = 260$, $a_e = 0.3$).

The trend of slight increasing of St_h with Re_h can be deduced also from two previous experimental works covering the domain of moderate Reynolds numbers. An increase of St_h from 0.1 to 0.18 was observed by Cherdron et al. [41] for Re_h changing from 250 to 800 in their aerodynamic tunnel with $ER = 2$. Fearn et al. [42] carried out LDA measurements in a water channel with a symmetric plane expansion of $ER = 3$ and found the values of St_h from 0.08 to 0.1 for the limited range of Re_h from 210 to 280.

As the Reynolds number is increased the global flow instability together with the effect of sidewalls makes the flow highly unsteady and 3D. The turbulent flow regime is then characterized by a complex spectrum of fluctuations, with the predominant frequency changing along the primary recirculation region. But still, if we extract from previous spectral data only those measured in close proximity of the reattachment zone, the characteristic Strouhal numbers obtained ($St_h \sim 0.14$ for $Re_h = 7500$ at $x/h = 9.5$ by Roos and Kegelman [17], $St_h \sim 0.13$ for $Re_h = 32\,500$ at $x/h = 8$ by Bhattacharjee et al. [15], $St_h \sim 0.14$ for $Re_h = 11\,000$ at $x/h = 7$ by Berbee and Ellzey [18], and $St_h \sim 0.14$ for $Re_h = 33\,000$ at $x/h = 8$ by Chun and Sung [22]) justify the scaling based on the step height.

3.2. Pulsatile flow at the inlet

The effect of pulsations imposed to the inlet flow on the laminar backward-facing step flow is documented in Fig. 11, where the time-average profiles of wall shear rate are presented for the different forcing frequencies applied at $Re_h = 260$. The shortening of primary recirculation zone and the intensification of reverse flow inside the recirculation zones are two distinct consequences of the inlet flow forcing. The strong flow inside the primary recirculation zone gives a rise of the corner eddy, which without forcing becomes considerable at much higher flow rates. The strongest effect of forcing, leading to the significant reduction of reattachment length, is observed at $f_e \sim 0.5$ Hz. As seen in Fig. 11(b), the roof eddy follows the flow rearrangement at the bottom wall by upstream shifting its location. It is obvious that imposed flow pulsations increase the fluctuating component of wall shear rate at all locations behind the step. In the case of laminar flow separation, the maximum value of $\bar{s}_w/s_{wo}$ magnifies forty times from 0.1 (for steady inlet flow) to 4 (for pulsatile inlet flow at $f_e \sim 0.5$ Hz).

If the time-averaged reattachment length is plotted against the forcing frequency (see Fig. 12), a symmetrical region of x_r/h reduction is observed around the most effective frequency of forcing f_{opt}. For the studied flow case, the maximum reduction of reattachment length (about 75%) is achieved for $f_{opt} \sim 0.45$ Hz. This frequency can be characterized by the Strouhal number of $St_{h,e} \sim 0.17$, hence the characteristic value, which is very close to that found out in the previous section for near-wall flow fluctuations under steady inlet flow conditions (St_h from 0.11 to 0.16).

Fig. 13 shows the result of experiments focused on the effect of forcing amplitude. For the same basic flow conditions ($Re_h = 260$), the forcing frequency is fixed at $f_{opt} = 0.45$ Hz and the wall shear rate profiles are measured for the different levels of forcing amplitude. The separation flow is very sensitive even to small amplitudes of forcing, e.g. 22% reattachment length reduction is achieved at $a_e = 0.03$. As the forcing amplitude is increased, the reattachment length is reduced more and more slowly. Finally, at high amplitudes ($a_e > 0.3$), the influence of forcing amplitude quickly saturates. The similar effect of forcing amplitude was observed also in the previous experiment by Yoshioka et al. [23].

The variation of the most effective forcing frequency with the Reynolds number is presented in Fig. 14. These results, which were obtained for moderate amplitudes of forcing (at $a_e = 0.1$), exhibit two distinct frequency branches probably originated from different modes of backward-facing step flow instability. The low-frequency branch dominates the laminar flow regime and its frequency approaches to the value of $f_{opt} \sim 0.5$ Hz at $Re_h \sim 500$. The Strouhal number values corresponding to this mode ($St_{h,e}$ between 0.15 and 0.11) suggest the forcing based on the frequency of the already mentioned "step mode" instability. However, the question is what scaling is appropriate to this instability mode. The recent stability analysis of low-Reynolds-number recirculation flows (see [12,14]) has provided the scaling for global perturbations with the maximum transient growth. These optimal perturbations were found to produce wave packets with the length scale proportional to the downstream channel height $\sim 2(H+h)$ and with the traveling velocity corresponding to the mean velocity far downstream $\sim U\{H/(H+h)\}$. The rescaling done for our expansion geometry with $ER = 2$ (thus $H = h$) gives an estimate $St_h \sim 1/8$, which is in a good agreement with our experimental values on $St_{h,e}$. It supports the hypothesis that at low

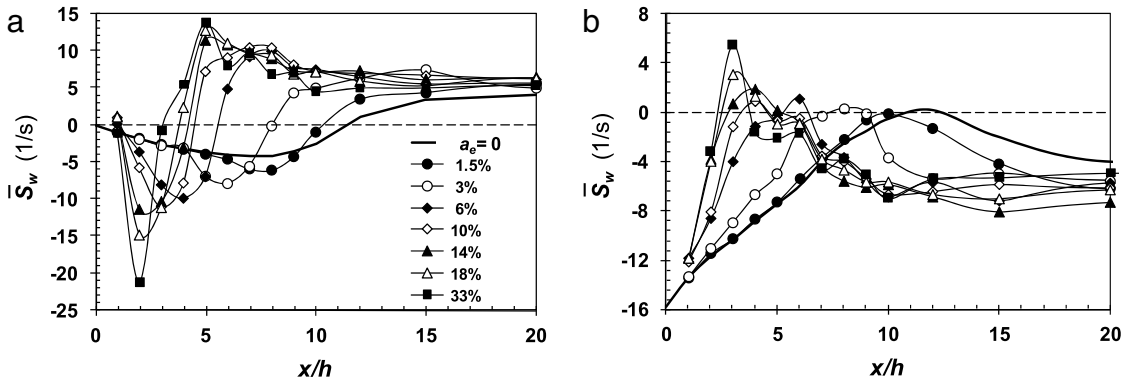

Fig. 13. Wall shear rate distributions measured for the different forcing conditions at (a) the bottom and (b) roof wall. The forcing amplitude a_e is varied at the constant forcing frequency $f_e = 0.45$ Hz; the same steady inlet flow conditions as in Fig.11 (i.e. $Re_h = 260$).

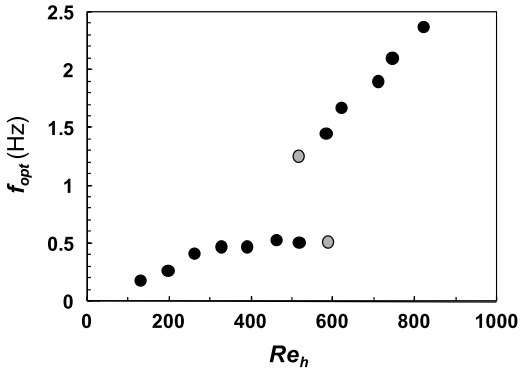

Fig. 14. Variation of the most effective forcing frequency with the Reynolds number.

Reynolds numbers (for $Re_h < 500$) the most effective forcing is achieved at the frequency promoting the global flow instability. On the other hand, the scaling for the high-frequency branch, which starts to prevail at the transient flow conditions (for $Re_h > 600$), is more obvious. Its frequency corresponds to the instability of "shear layer mode" and the characteristic value of $St_{\theta,e} \sim 0.011$ is obtained by using the scaling based on the momentum thickness θ and the maximum inlet velocity $U_{\max}$ (both these parameters are calculated for the laminar velocity profile developed in the inlet channel section). The grey circles are used in Fig. 14 to indicate the mode which is still important but already or not yet dominant.

The competition between two instability modes observed under moderate Re_h is demonstrated in Fig. 15. The "shear layer mode" is first more effective only at small forcing amplitudes (see Fig. 15(a)), then as the Reynolds number is increased it quickly becomes dominant over the whole amplitude range (see Fig. 15(c)).

The wall shear rate distributions measured for the flow forcing under transient flow conditions are presented in Fig. 16. In this case ($Re_h = 720$, $a_e = 0.2$, corresponding to the situation shown in the middle part of Fig. 15(b)), two distinct forcing modes provide the same reduction of the reattachment length (see the crossings with the $\bar{s}_w = 0$ line in Fig. 16(a). Nevertheless, the near-wall flows induced by these two forcing modes are quite different. The forcing at the "step mode" leads to the flow characterized by strong pulsations (see large values of $\tilde{s}_w$ corresponding to the reattachment region in Fig. 16(b)). The pulsatile character of the near-wall flow with large oscillations of the reattachment position can be also deduced from the reverse-flow diagram in Fig. 16(c). Due to gradual changes of γ_p observed in the region of $x/h < 10$, the boundaries between the individual recirculation flow zones are not sharply delimited. In contrast, the forcing at the "shear layer mode" induces the flow whose character is much more similar to that observed under steady inlet flow conditions. The fluctuating component of wall shear rate is just slightly elevated and the slope of γ_p-distribution around reattachment has similar steepness as in the case of steady inlet flow. Different character of near-wall flow fluctuations is reflected also in Fig. 16(d), where the power spectra obtained at different forcing conditions are compared. The spectra are calculated from data measured just behind the mean reattachment points, thus at the locations of $\tilde{s}_{w,\max}$, which are indicated in Fig. 16(b) with arrows. The spectra differentiate mainly at low frequencies (for $f < 1$ Hz). The forcing at $f_e = 1.9$ Hz ("shear layer mode") increases spectral values quite uniformly over whole low-frequency range, whereas in the case forcing at $f_e = 0.54$ Hz ("step mode") this increase is concentrated mainly into the peak observed at $f = f_e$.

Fig. 17 shows the power spectra of wall shear rate fluctuations obtained for the steady inlet flow conditions. The spectra are

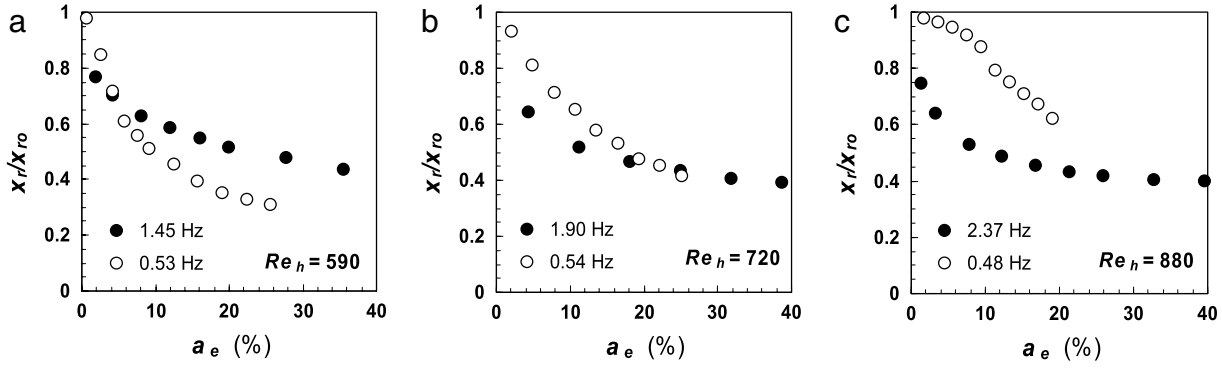

Fig. 15. Dependence of the reattachment length on the forcing amplitude for two effective frequency modes: "shear mode" (solid circles) and "step mode" (open circles), (a) $Re_h = 590$, (b) $Re_h = 720$, and (c) $Re_h = 880$.

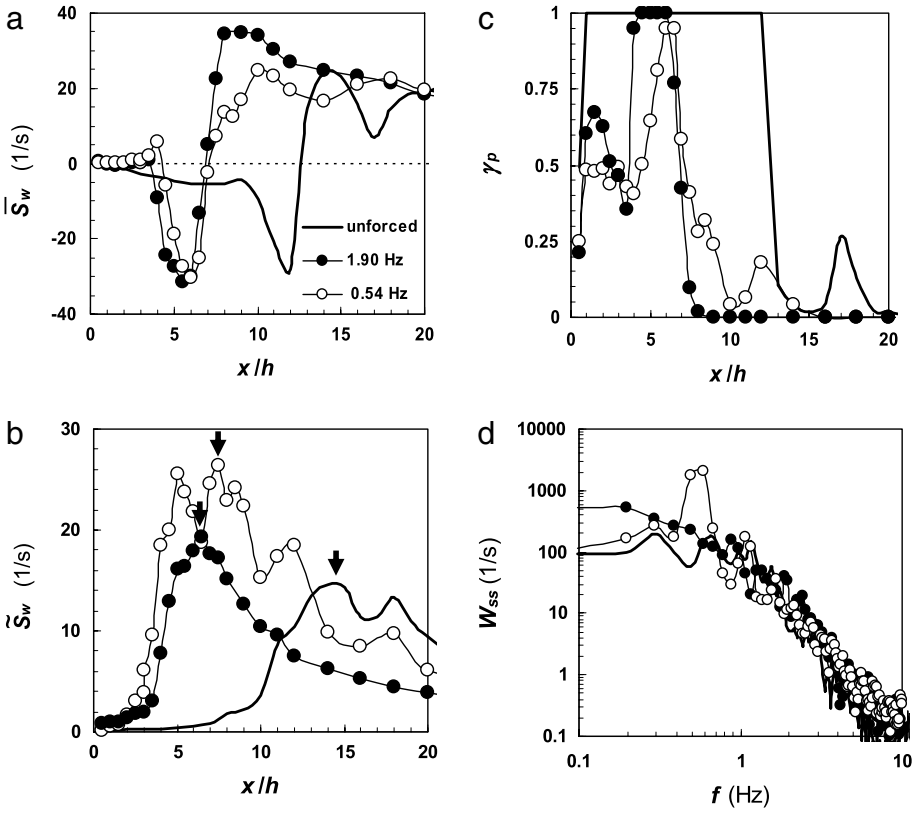

Fig. 16. Wall shear rate distributions measured at the bottom wall under three forcing conditions ($f_e = 0$, 0.54, 1.9 Hz, $a_e = 0.3$, $Re_h = 720$): (a) time-averaged values, (b) fluctuation (r.m.s) magnitude, (c) reverse-flow time fraction, (d) power spectra calculated from data measured at the $\tilde{s}_{w,\max}$ locations (see the arrows in Fig. 16(b).

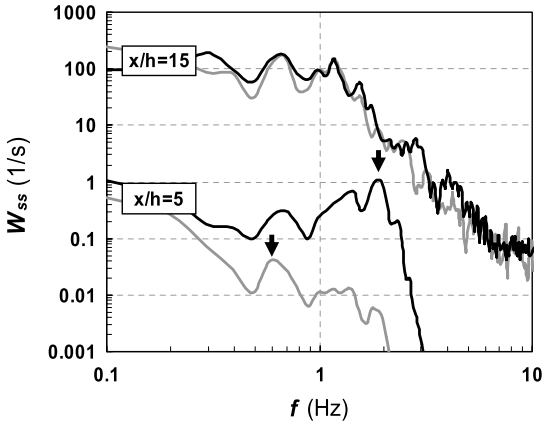

Fig. 17. Power spectra of wall shear rate fluctuations measured for steady inlet flow conditions ($Re_h = 720$) at the bottom (grey lines) and roof (black lines) wall.

calculated from the time signals measured by both probes (bottom and roof wall) at two locations ($x/h = 15$: downstream the reattachment point, $x/h = 5$: upstream the reattachment point). The same level of near-wall fluctuations is observed at the bottom and roof wall downstream the reattachment point, where both the spectra exhibit a short low-frequency plateau. On contrary the spectra provided for $x/h = 5$ are characterized by two distinct peaks: the first one (at the bottom wall, inside the flow-recirculation region) corresponds to the "step mode" instability, the second one (at the roof wall, above the free shear layer) to the "shear layer mode" instability.

As the Reynolds number is changing, the reduction of reattachment length with the forcing amplitude has different steepness. The strongest effect of forcing is observed at moderate flow rates, when the flow is very sensitive to perturbations and long recirculation regions are easy to reduce. The values of x_r/h obtained for the most effective forcing are plotted in Fig. 18(a) and rescaled in Fig. 18(b) with respect to the time-averaged reattachment length x_{ro} (obtained for steady inlet flow conditions, thus for $a_e = 0$). The maximum reduction of the reattachment length is achieved for Re_h ranging from 300 to 500. The value of x_r/h drops below 3 and the relative reduction of x_{ro} approaches 80%. As Re_h is decreased (towards the laminar regime) or increased (towards the turbulent regime), the effect of forcing on the reattachment length becomes gradually weaker.

4. Conclusions

The application of the electrodiffusion technique provides valuable information on the near-wall flow in a backward-facing step configuration ($ER = 2$) over a wide range of inlet flow conditions (Re_h ranging from 30 to 1800, f_e from 0 to 3 Hz, a_e from 0 to 0.5):

The near-wall extent of primary (mean reattachment length) and secondary (corner and roof eddy location) recirculation zones is determined from the inspection of unsteady wall shear rate profiles measured at both, the bottom and roof wall. The Reynolds number dependence of the reattachment length with two distinct values ($x_{r,\max}/h \sim 16$ and $x_{r,turb}/h \sim 7$) is obtained. The inception (at $Re_h \sim 230$) and temporary existence of the roof eddy brings about rapid destabilization of the flow. The small corner eddy, which is predicted to exist even at low Reynolds numbers, becomes experimentally detectable at moderate Reynolds numbers. Under transient flow conditions it quickly expands and its length achieves a value of $x_c/h \sim 2.5$ at turbulent flow conditions, when the ratio of characteristic lengths stabilizes at a value of $x_c/x_r \sim 1/3$.

The high magnitude of skin friction inside of the primary recirculation zone is strongly Reynolds-number dependent. The large changes in the reattachment length at moderate Reynolds numbers affect the flow redistribution at the reattachment point.

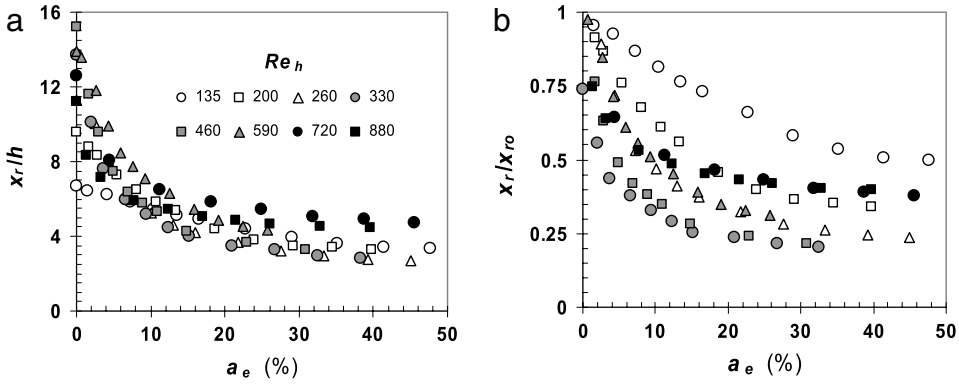

Fig. 18. Reduction of the reattachment length achieved for the most effective forcing at the different Reynolds numbers (for the particular values of forcing frequency inspect Fig. 14).

Consequently, the $c_{f,\min}(Re)$ curve changes its shape in the transient flow region. The negative peak on the wall shear rate profile changes its localization in respect to the reattachment point as well. At low flow rates it is placed in the middle of primary recirculation zone ($x_p/x_r \sim 0.5$), then is shifted towards the reattachment ($x_p/x_r \sim 0.9$ for Re_h ranging from 650 to 850), and finally is moved back upstream and stabilized at the position of $x_p/x_r \sim 2/3$ under turbulent flow conditions.

The magnitude of velocity fluctuations in the near-wall region is of the order of local mean velocity already at moderate Reynolds numbers. The position of maximum wall shear rate fluctuations is first (in laminar regime) located in the region of redeveloping channel flow, then (in transient regime) shifted just behind the reattachment, and finally (in turbulent regime) found in front of the reattachment point. The spectral analysis reveals that the low-frequency fluctuations characterized by $St_h \sim 0.15$ dominate the reattachment region under steady inlet flow conditions.

The pulsations superimposed to the inlet flow strongly affect the structure of backward-facing step flow. The vortices are forming closer to the step, the process of vortex rolling-up becomes more regular, and consequently the size of the primary recirculation zone is reduced. The roof eddy follows the changes in flow rearrangement behind the step and also shifts its location upstream. At the same time it becomes shorter and the reverse flow inside stronger. The corner eddy becomes more significant as well.

If the most effective frequency is applied for forcing, the reattachment length reduction with a level up to 80% can be achieved. Two flow instability modes are found to control this frequency: the "step mode" dominates the laminar flow regime, whereas the "shear layer mode" prevails at the transient flow conditions. The frequency of "step mode" coincides with the scaling recently suggested for the global instability of backward-facing step flows. Although these two distinct modes of forcing can produce at certain operation conditions the same shortening of reattachment length, the character of near-wall flow induced by them is qualitatively different.

Acknowledgement

This work was supported by the Grant Agency of the Czech Republic (under the projects, Nos 101/04/0745 and 104/08/0428) and by the European Commission (in the frame of MCTS programme HPMT-CT-2000-00074). Dr. J. Havlica is acknowledged for performing the numerical calculations.

References

[1] B.F. Armaly, F. Durst, J.C.F. Pereira, B. Schönung, Experimental and theoretical investigation of backward-facing step flow, J. Fluid Mech. 127 (1983) 473–496.
[2] B.F. Armaly, A. Li, J.H. Nie, Measurements in three-dimensional laminar separated flow, Int. J. Heat Mass Transfer 46 (2003) 3573–3582.
[3] J.H. Nie, B.F. Armaly, Reverse flow regions in three-dimensional backward-facing step flow, Int. J. Heat Mass Transfer 47 (2004) 4713–4720.
[4] P.T. Williams, A.J. Baker, Numerical simulations of laminar flow over a 3D backward-facing step, Internat. J. Numer. Methods Fluids 24 (1997) 1159–1183.
[5] T.P. Chiang, T.W.H. Sheu, A numerical revisit of backward-facing step flow problem, Phys. Fluids 11 (1999) 862–874.
[6] G. Biswas, M. Breuer, F. Durst, Backward-facing step flows for various expansion ratios at low and moderate Reynolds numbers, J. Fluids Eng. 126 (2004) 362–374.
[7] A. Kitoh, K. Sugawara, H. Yoshikawa, T. Ota, Expansion ratio effects on three-dimensional separated flow and heat transfer around backward-facing steps, J. Heat Transfer 129 (2007) 1141–1155.
[8] L. Kaiktsis, G.E. Karniadakis, S.A. Orszag, Onset of three-dimensionality, equilibria, and early transition in flow over a backward-facing step, J. Fluid Mech. 231 (1991) 501–528.
[9] D. Barkley, M.G.M. Gomes, R.D. Henderson, Three-dimensional instability in flow over a backward-facing step, J. Fluid Mech. 473 (2002) 167–190.
[10] J.-F. Beaudoin, O. Cadot, J.-L. Aider, J.E. Wesfreid, Three-dimensional stationary flow over a backward-facing step, Eur. J. Mech. B Fluids 23 (2004) 147–155.
[11] V. Theofilis, S. Hein, U. Dallmann, On the origin of unsteadiness and three-dimensionality in a laminar separation bubble, Philos. Trans. R. Soc. Lond. A 358 (2000) 3229–3246.
[12] H.M. Blackburn, D. Barkley, S.J. Sherwin, Convective instability and transient growth in flow over a backward-facing step, J. Fluid Mech. 603 (2008) 271–304.
[13] U. Ehrenstein, F. Gallaire, Two-dimensional global low-frequency oscillations in a separating boundary-layer flow, J. Fluid Mech. 614 (2008) 315–327.
[14] O. Marquet, D. Sipp, J.M. Chomaz, L. Jacquin, Amplifier and resonator dynamice of a low-Reynolds-number recirculation bubble in a global framework, J. Fluid Mech. 605 (2008) 429–443.
[15] S. Bhattacharjee, B. Scheelke, T.R. Troutt, Modification of vortex interactions in a reattaching separated flow, AIAA J. 24 (1986) 623–629.
[16] M.A.Z. Hasan, The flow over a backward-facing step under controlled perturbation: Laminar separation, J. Fluid Mech. 23 (1992) 73–96.
[17] F.W. Roos, J.T. Kegelman, Control of coherent structures in reattaching laminar and turbulent shear layers, AIAA J. 24 (1986) 1956–1963.
[18] J.G. Berbee, J.L. Ellzey, The effect of aspect ratio on the flow over a rearward-facing step, Exp. Fluids 7 (1989) 447–452.
[19] D. Wee, T. Yi, A. Annaswamy, A.F. Ghoniem, Self-sustained oscillations and vortex shedding in backward-facing step flows: Simulation and linear instability analysis, Phys. Fluids 16 (2004) 3361–3373.
[20] I. Lee, H.J. Sung, Characteristics of wall pressure fluctuations in separated and reattaching flows over a backward-facing step: Part I. Time-mean statistics and cross-spectral analyses, Exp. Fluids 30 (2001) 262–272.
[21] K. Isomoto, S. Honami, The effect of inlet turbulence intensity on the reattachment process over a backward-facing step, J. Fluids Eng. 111 (1989) 87–92.
[22] K.B. Chun, H.J. Sung, Control of turbulent separated flow over a backward-facing step by local forcing, Exp. Fluids 21 (1996) 417–426.
[23] S. Yoshioka, S. Obi, S. Masuda, Organized vortex motion in periodically perturbed turbulent separated flow over a backward-facing step, Int. J. Heat Fluid Flow 22 (2001) 301–307.
[24] S. Kang, H. Choi, Suboptimal feedback control of turbulent flow over a backward-facing step, J. Fluid Mech. 463 (2002) 201–227.
[25] A. Dejoan, M.A. Leschziner, Large eddy simulation of periodically perturbed separated flow over a backward-facing step, Int. J. Heat Fluid Flow 25 (2004) 581–592.
[26] J. Dandois, E. Garnier, P. Sagaut, Numerical simulation of active separation control by a synthetic jet, J. Fluid Mech. 574 (2007) 25–58.
[27] K.B. Chun, H.J. Sung, Visualization of a locally-forced separated flow over a backward-facing step, Exp. Fluids 25 (1998) 133–142.

[28] H. Wengle, A. Huppertz, G. Baerwolff, G. Janke, The manipulated transitional backward-facing step flow: an experimental and direct numerical simulation investigation, Eur. J. Mech. B Fluids 20 (2001) 25–46.
[29] T.J. Hanratty, J.A. Campbell, Measurement of wall shear stress, in: J.R. Goldstein (Ed.), Fluid Mechanics Measurement, Hemisphere, Washington, 1983, pp. 559–615.
[30] J. Tihon, V. Tovchigrechko, V. Sobolik, O. Wein, Electrodiffusion detection of the near-wall flow reversal in liquid films at the regime of solitary waves, J. Appl. Electrochem. 33 (2003) 577–587.
[31] T. Lee, D. Mateescu, Experimental and numerical investigation of 2D backward-facing step flow, J. Fluid Struct. 12 (1998) 703–716.
[32] S. Thangam, D.D. Knight, Effect of stepheight on the separated flow past a backward facing step, Phys. Fluids A 1 (1989) 604–606.
[33] H. Iwai, K. Nakabe, K. Suzuki, Flow and heat transfer characteristics of backward-facing step laminar flow in a rectangular duct, Int. J. Heat Mass Transfer 43 (2000) 457–471.
[34] N. Kasagi, A. Matsunaga, Three-dimensional particle-tracking velocimetry measurement of turbulence statistics and energy budget in a backward-facing step flow, Int. J. Heat Fluid Flow 16 (1995) 477–485.
[35] J. Tihon, J. Legrand, P. Legentilhomme, Near-wall investigation of backward-facing step flows, Exp. Fluids 31 (2001) 484–493.
[36] P.G. Spazzini, G. Iuso, M. Onorato, N. Zurlo, G.M. Di Cicca, Unsteady behavior of back-facing step flow, Exp. Fluids 30 (2001) 551–561.
[37] C. Schram, P. Rambaud, M.L. Riethmuller, Wavelet based eddy structure eduction from a backward facing step flow investigated using particle image velocimetry, Exp. Fluids 36 (2004) 233–245.
[38] H. Le, P. Moin, J. Kim, Direct numerical simulation of turbulent flow over a backward-facing step, J. Fluid Mech. 330 (1997) 349–374.
[39] K.F. Yu, K.S. Lau, C.K. Chan, Numerical simulation of gas-particle flow in a single-side backward-facing step flow, J. Comp. Appl. Math. 63 (2004) 319–331.
[40] C. Benocci, R. Giammanco, M. Manna, E. Simons, Large eddy simulation of turbulent flows via domain decomposition techniques, Internat. J. Numer. Methods. Fluids 48 (2005) 397–422.
[41] W. Cherdron, F. Durst, J.H. Whitelaw, Asymmetric flows and instabilities in symmetric ducts with sudden expansions, J. Fluid Mech. 84 (1978) 13–31.
[42] R.M. Fearn, T. Mullin, K.A. Cliffe, Nonlinear flow phenomena in a symmetric sudden expansion, J. Fluid Mech. 211 (1990) 595–608.